

## A CONCATENATED UP AND DOWN TAPERED FIBER FOR SIMULTANEOUS MEASUREMENT OF STRAIN AND TEMPERATURE

Mustafa BILSEL and Isa NAVRUZ

Ankara University, Faculty of Engineering, Department of Electrical and Electronics  
Engineering, Ankara, TURKEY

**ABSTRACT.** A novel fiber optical sensor based on in-line fiber Mach-Zehnder interferometer for simultaneous measurement of strain and temperature is proposed and demonstrated experimentally. The interferometer is simple, extremely robust and highly sensitive and consists of two concatenated parts; one is a down-tapered fiber (DTF) and the other is an up-tapered fiber (UTF). UTF and DTF sections of the sensor are fabricated by using a commercial fiber splicer and a non-commercial setup based on heating and stretching a portion of a standard single-mode fiber, respectively. While UTF section behaves as a beam splitter to decompose the injected light into core and cladding modes, DTF section provides evanescent field to access the surrounding environment. Experimental results indicate that the resolutions of 0.83 °C and 45.80  $\mu\epsilon$  were achieved in temperature and strain, respectively, for simultaneous measurement with a 10 pm of wavelength resolution.

### 1. INTRODUCTION

Simultaneous strain and temperature measurement ability of optical fiber sensors has attracted great attention in many research areas due to its importance in the fields such as environmental inspection, real-time structural health monitoring, tracing deformation in civil/mechanical engineering and aerospace industry. To satisfy distinct response to strain and temperature, these sensors usually include hybrid configurations or special type of fibers in their structure. Researchers have presented many techniques based on FBG, LPG, all-fiber Mach-Zehnder interferometer (MZI), special fiber assisted and their combinations. Recently, a broad range of devices and configurations have been investigated such as splicing FBG with multimode fiber and sandwiching them between two single mode fibers (SMFs) [1], combining FBG with a multimode fiber [2], splicing two FBGs written with different

*Keyword and phrases.* Up-tapered fiber, down-tapered fiber, simultaneous measurement, strain, temperature.

 mfbilsel@gmail.com -Corresponding author; inavruz@ankara.edu.tr  
 0000-0001-8252-3734;0000-0003-2976-076X

diameters [3], inscribing micro tapers on a slightly tapered fiber by using filament heating method [4], periodically micro-tapered fiber grating [5], using S tapered fiber embedded in FBG [6], cascading an LPG and a polarization maintaining fiber loop mirror [7] and combining an LPG with a high-birefringence fiber loop mirror [8]. Although these sensor structures accomplish adequate sensitivity in responding to strain and sensitivity, complex structure and fragility limit their use in potential applications. On the other side, special type of fiber-assisted MZIs have been fabricated such as an air-cavity embedded in a slightly tapered fiber via femtosecond laser [9], concatenating two up-taper fibers (UTF) [10], splicing a thin core fiber between two standard single-mode fibers and acting a core offset in one side of the thin core fiber [11], tapering a coreless multimode fiber as a sensing head [12] and Z-shape structure fabricated by exposing CO<sub>2</sub> laser on a single mode fiber [13]. However, their cost effectiveness is not satisfied owing to complicated fabrication and dependency on particular fiber type.

In this letter, we propose an all-fiber sensor formed by concatenating a UTF and a DTF joint. UTF structure was fabricated by using a commercial fusion splicer via splicing through setting the overlap parameter without changing the other splicing parameters. DTF structure was fabricated by using electrical arc discharge method in which a section of fiber was stretched while heating it up to its softening point so that diameters of both core and cladding decrease dramatically. In electrical arc discharge method, effective heat zone of electrodes is large so adiabaticity of DTF is adversely affected. For this reason, DTF sensors are required to be fabricated with small waist diameters to obtain a transmission spectrum with high fringe visibility. Practically, to get through the issue of thin waist diameter, UTF joint is a good choice and can impressively excite higher order cladding modes by satisfying the adiabaticity criteria. High-order cladding modes are generated when light interacts with UTF region because of the mismatch of the mode field diameter and it leads light to decompose into two parts, one propagating in the core and the other in the cladding of the fiber. Light confined between the taper region of DTF and surrounding medium can penetrate the surrounding environment in the form of evanescent wave. Changes in the conditions of the environment result in a wavelength shift in output interference spectrum as a function of surrounding parameters such as temperature, strain or refractive index.

## 2. SENSOR FABRICATION AND PRINCIPLE

Microscope captured images of the fabricated UTF and DTF are shown in Figure 1-(a) and (b), respectively. The proposed sensor structure is composed of two parts; leading UTF and subsequent DTF joint. Leading UTF is fabricated by using a commercial fiber splicer (Fujikura FSM-60s) in built-in mode by setting the overlap distance which is a measure of coincidence between two cleaved fiber ends when they pushed towards each other. To decompose fundamental mode into cladding modes and acquire interference spectrum with

desired free spectral range (FSR), maximum overlap distance of  $150\ \mu\text{m}$  was chosen without changing the other splicing parameters. In splicing process, two stripped and cleaved fiber tips become softened and then push towards each other when electrodes are discharged so a gradually enlarged fiber diameter like a plump fiber is formed. Standard cladding diameter of  $125\ \mu\text{m}$  was increased to about  $165\ \mu\text{m}$ . It generated an insertion loss of 9.6-12.7 dB when only UTF joint was applied to SMF. It means that about 90-95% of the total input power is coupled into cladding modes, 5-10% of optical power still remains propagating in the core mode.

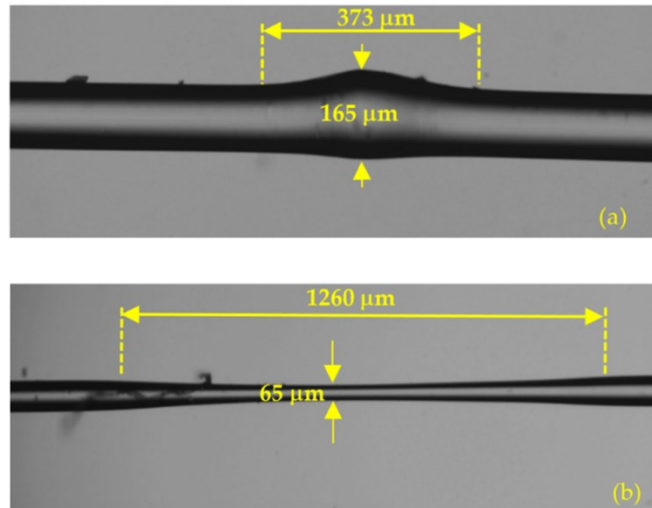


FIGURE 1. Microscopic image of (a) UTF and (b) DTF.

DTF joint of the proposed sensor was produced in our setup in Figure 2. We have also used the same setup in our experiments and it has also worked successfully to generate a DTF in our previous work [14]. Firstly, protective coating of a section of SMF was stripped and one end of the fiber was fixed with left fiber holder. The other end of the fiber is placed on right fiber holder whose motion is controlled by a stepper motor with a resolution of  $1.25\ \mu\text{m}$  axial motion at each step. Secondly, a series of arc pulses are applied for a short time via electrodes to reach the softening point of the fiber and pulse duration is decreased to 80% of its maximum level. Then, steppers start to move in opposite direction; one stretching the fiber with a higher speed (stepper motor on the right) and the other moving the electrodes with a lower speed (stepper motor on the left). Acceleration and speed of fiber holders, pulse duration and instantaneous arc power are controlled by a computer software. Desired waist diameter and length of the taper can be adjusted by choosing suitable parameters in the

software. One of the major advantage of our setup compared to the commercial fusion splicer is no restriction on waist diameter and length. So, a tapered fiber section that one wishes to fabricate can be acquired with such a computer controlled setup. In the experiments, UTF joint has been initially fabricated, then DTF joint has been located at a distance of about 2 cm away from UTF. Wavelength spectrum is directly affected from the waist diameter so it is crucial to reproduce a sensor with the same geometry. To evaluate the reproducibility, 10 samples were fabricated with waist diameter of 65  $\mu\text{m}$  and relative standard deviation was calculated as 1.8%. It is important to note that precise measurement of waist diameter from microscopic image also affects reproducibility.

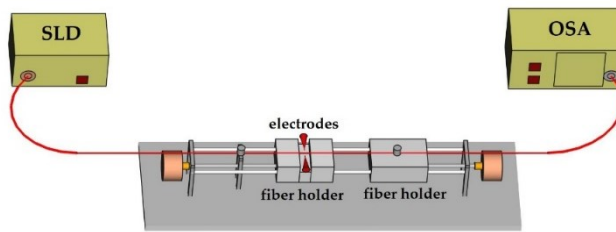
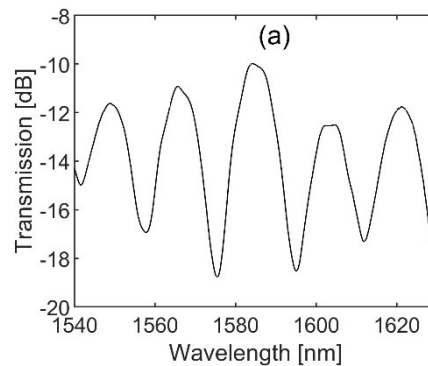


FIGURE 2. Experimental setup for fabrication of DTF.

At room temperature, typical transmission spectrum of the proposed sensor in air was shown in Figure 3-(a). Maximum extinction ratio for the dip located at 1575.5 nm is 8.7 dB. To investigate the cladding modes that contribute the interference spectrum, the Fourier transform was performed and the related spatial frequency spectrum was shown in Figure 3-(b). It indicates that only one cladding mode has been stimulated and contributed to the interference spectrum.



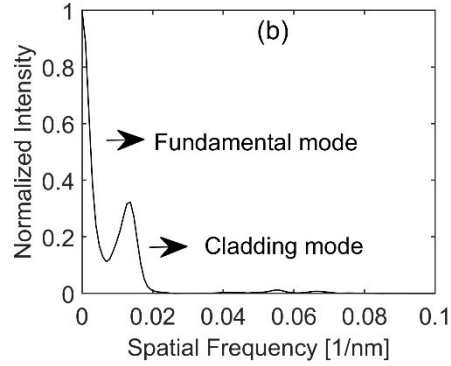


FIGURE 3. (a) Typical spectrum at room temperature in air and (b) its Fourier transform.

Assuming only one core mode is excited, then output intensity of MZI can be expressed as [15],

$$I = I_{co} + I_{cl} + 2\sqrt{I_{co}I_{cl}}\cos\varphi \quad (1)$$

where  $I$  is the intensity of throughput,  $I_{co}$  and  $I_{cl}$  are the intensities of core and cladding modes, respectively, and  $\varphi$  is the phase difference between core and cladding modes. Due to difference in refractive index of core and any cladding mode, a phase difference between them occurs:

$$\varphi = \frac{2\pi\Delta n_{eff}L}{\lambda} \quad (2)$$

where  $\Delta n_{eff}$  is the effective refractive index difference between core and cladding modes,  $L$  is the length of the sensor and  $\lambda$  is the wavelength of the light. When phase difference becomes equal to odd-multiple of  $\pi$ , that is,  $\varphi = (2m+1)\pi$ , where  $m$  is an integer, destructive interference occurs and dip points in interference spectrum is observed. Dip wavelength of the  $m$ -th order cladding mode in interference spectrum can be expressed as:

$$\lambda_{dip} = \frac{2\Delta n_{eff}L}{2m+1} \quad (3)$$

Differentiating Eq. (3) with respect to temperature,  $T$ , yields temperature dependency of dip wavelength:

$$\frac{\partial \lambda_{dip}}{\partial T} = \frac{2}{2m+1} \left[ \Delta n_{eff} \frac{\partial L}{\partial T} + L \left( \frac{\partial n_{eff}^{co}}{\partial T} - \frac{\partial n_{eff}^{cl}}{\partial T} \right) \right] \quad (4)$$

where the first term in squared brackets,  $\partial L/\partial T$ , is thermal-expansion coefficient of silica which represents the variation of sensor length with temperature, and the second term,  $\frac{\partial n_{eff}^{co}}{\partial T} - \frac{\partial n_{eff}^{cl}}{\partial T}$  is thermo-optical coefficient of silica which denotes the change in refractive index of both core and cladding with respect to temperature. For silica, thermal-expansion and thermo-optic coefficients are  $0.55 \times 10^{-6} / ^\circ\text{C}$  and  $8.0 \times 10^{-6} / ^\circ\text{C}$  [16], respectively, which means thermo-optic coefficient is the dominant term in the case of temperature variation. Similarly, response of dip wavelength to applied strain can be expressed as,

$$\frac{\partial \lambda_{dip}}{\partial \varepsilon} = \frac{2}{2m+1} \left[ \Delta n_{eff} \frac{\partial L}{\partial \varepsilon} + L \left( \frac{\partial n_{eff}^{co}}{\partial \varepsilon} - \frac{\partial n_{eff}^{cl}}{\partial \varepsilon} \right) \right] \quad (5)$$

where  $\varepsilon$  is the applied strain. According to the equation, both length and refractive index of refraction are affected from strain due to elasto-optical effect. Strain can be defined as [17],

$$\varepsilon = \frac{\Delta L}{L} \quad (6)$$

where  $L$  is initial length and  $\Delta L$  is the change in length.

Simultaneous measurement of strain and temperature can be investigated by monitoring wavelength shift of two dips. Coefficient matrix [11] which includes experimentally calculated sensitivities and wavelength shifts can be used to find the resolution of the sensor in simultaneous strain and temperature measurement:

$$\begin{bmatrix} \Delta \lambda_A \\ \Delta \lambda_B \end{bmatrix} = \begin{bmatrix} S_{T,A} & S_{\varepsilon,A} \\ S_{T,B} & S_{\varepsilon,B} \end{bmatrix} \begin{bmatrix} \Delta T \\ \Delta \varepsilon \end{bmatrix} \quad (7)$$

where  $\Delta \lambda_A$  and  $\Delta \lambda_B$  are the wavelength shifts;  $S_{T,A}$ ,  $S_{T,B}$  are temperature sensitivities;  $S_{\varepsilon,A}$ ,  $S_{\varepsilon,B}$  are strain sensitivities of dipA and dipB, respectively.  $\Delta T$  and  $\Delta \varepsilon$  are variations of ambient temperature and applied strain, respectively.

### 3. RESULTS AND DISCUSSION

To characterize the proposed MZI sensor, light from a superluminescent diode (SLD) source with a range of 1450-1650 nm was injected to the sensor and the interference spectrum was recorded by an optical spectrum analyzer (Thorlabs OSA-202) with a maximum resolution of 30 pm. For strain measurements, same setup in Figure 2 was used without operating electrodes, that is, when one end of the MZI was fixed with left fiber holder, the other end was clamped on right fiber holder. Each time right stepper was moved a particular distance an external force was acted on fiber. Referring to Figure 3-(a), the resonant dips named as

dipA, dipB and dipC located at 1575.5, 1595.2, 1611.8 nm were followed for strain and temperature measurements. Due to cross-sensitivity temperature was kept constant during strain measurements and vice versa. Transmission spectrum of the proposed sensor with different strain was shown in Fig. 4-(a). Resonant dips showed blue-shift when strain values were increased from 0  $\mu\epsilon$  to 1430  $\mu\epsilon$ . To avoid possible errors in calculating sensitivity, it should be assured that dips do not include ripples. For this reason, enlarged views of all dips were plotted in Figure 5. According to the figure, total shift in dipA, dipB and dipC was 1.5 nm, 1.4 nm and 0.9 nm, respectively. Signal variation in dip points is due to type of cladding modes excited. It indicates that dipC is less sensitive to strain, thereby it is thought dipC is resulted from UTF joint. Variation of dip points with respect to applied strain was analyzed by linear fitting. The corresponding sensitivities of dipA, dipB and dipC to strain were calculated as 1.00 pm/ $\mu\epsilon$ , 0.95 pm/ $\mu\epsilon$  and 0.69 pm/ $\mu\epsilon$ , respectively as shown in Figure 4-(b). The correlation coefficient values ( $R^2$ ) higher than 0.99 were achieved, which exhibited good linear response. Assuming an OSA with 10 pm wavelength resolution, the proposed sensor can achieve strain resolution of 9.90  $\mu\epsilon$  for dipA in discrete strain measurements.

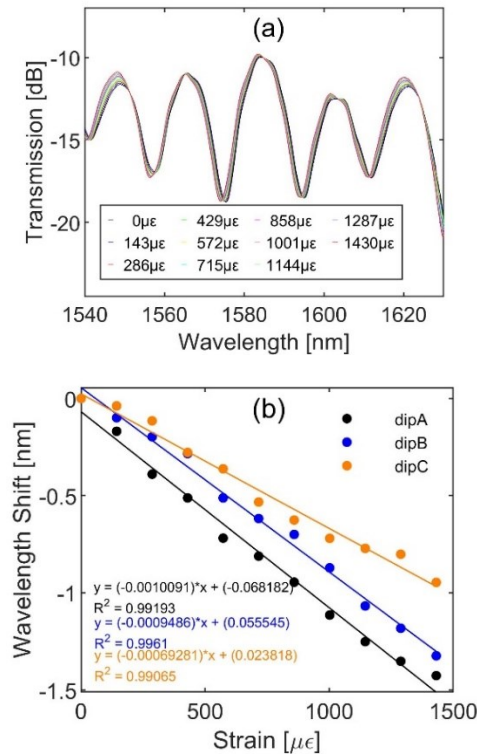


FIGURE 4. (a) Transmission spectrum with different strain and (b) wavelength shift of dip points versus tensile strain.

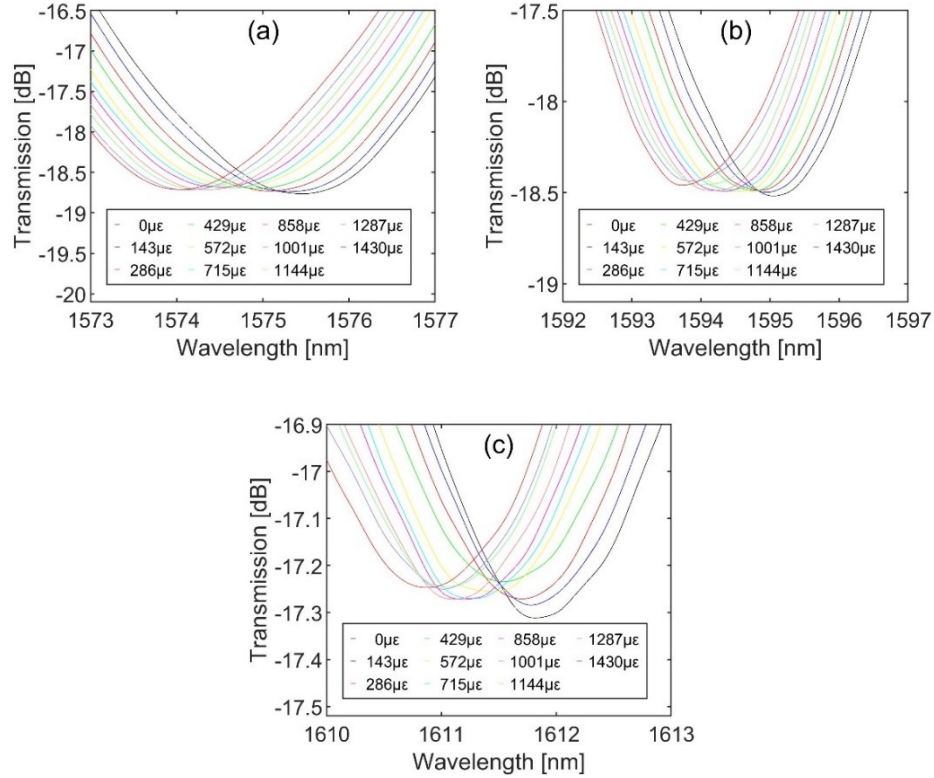


FIGURE 5. Enlarged views of (a) dipA, (b) dipB and (c) dipC.

In temperature measurements, a proportional-integral-derivative (PID) controlled furnace manufactured in our laboratory was used. Resistive element with power of 300 W was placed in the furnace and its power control was achieved with a commercial temperature controller (ENDA ETC4420). Inner temperature of the furnace can be set with an accuracy of  $\pm 0.1$   $^{\circ}\text{C}$  and the temperature was measured by a calibrated temperature probe (Testo 100) with a resolution of 0.1  $^{\circ}\text{C}$ . To keep the strain constant during temperature measurements, sensor was flattened on an aluminium plate placed in the furnace. When temperature was increased in the range of 21-65  $^{\circ}\text{C}$ , all the dips exhibited red-shift as shown in Figure 6-(a). According to the figure, dipC with total shift of 2.3  $\mu\text{m}$  was experienced the highest response to temperature variation although its response to strain was low. This result verified the origin of dipC and we infer that it is due to the UTF joint. As shown in Figure 6-(b), temperature

sensitivities of 41.92 pm/°C, 40.01 pm/°C and 49.92 pm/°C were acquired for dipA, dipB and dipC, respectively. The correlation coefficient greater than 0.99 shows good linearity in measurements. Temperature resolution of 0.2 °C in discrete temperature measurements can be achieved by following dipC for 10 pm wavelength resolution.

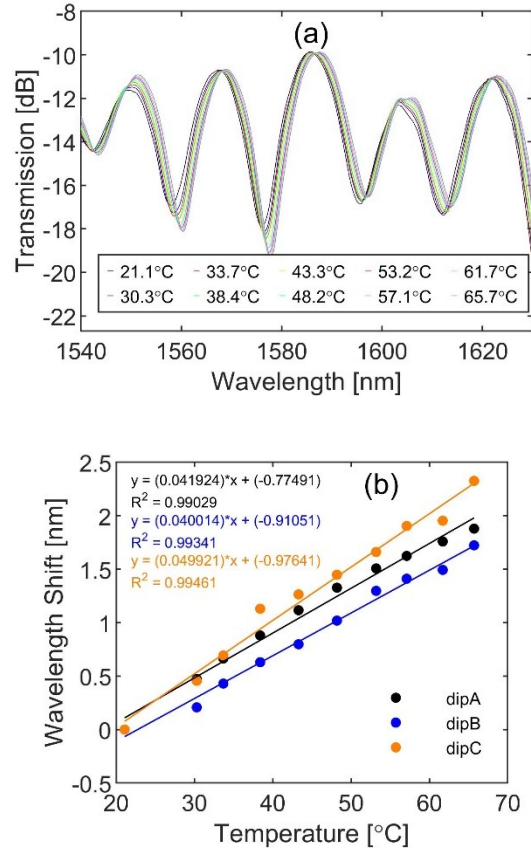


FIGURE 6. (a) Transmission spectrum with different temperature and (b) wavelength shift of dip points versus temperature.

Under the same experimental conditions, strain and temperature measurements repeated 3 times to investigate the repeatability. Resultant strain and temperature sensitivity plots for dipA were shown in Fig. 7.a and Fig. 7.b, respectively. Relative standard deviations in three measurements were calculated as 0.8% and 2.1% for strain and temperature, respectively. Calculations for dipB and dipC had similar results with dipA. It means that the proposed sensor has good repeatability.

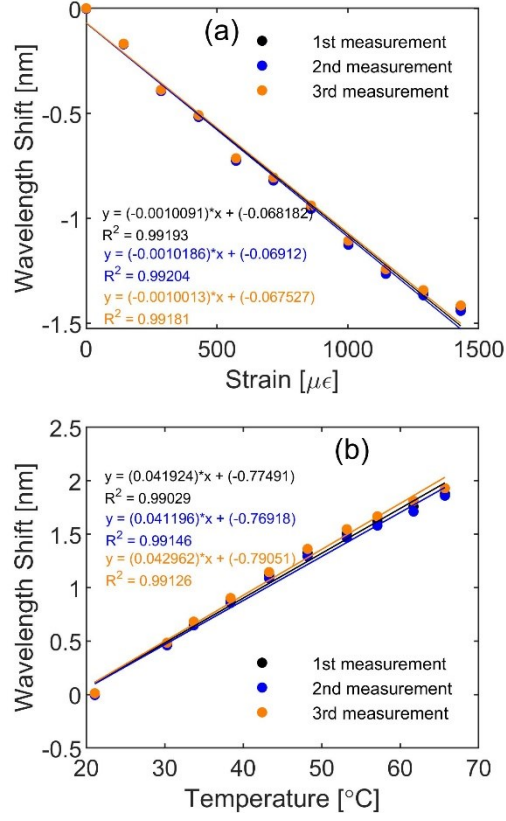


FIGURE 7. Reiterated experiments of (a) strain and (b) temperature.

By using sensitivity values obtained from experimental results, coefficient matrix introduced in Eq. 7 can be written to find the resolution of the proposed sensor for simultaneous measurement of strain and temperature:

$$\begin{bmatrix} \Delta\lambda_B \\ \Delta\lambda_C \end{bmatrix} = \begin{bmatrix} 40.014 & -0.9486 \\ 49.921 & -0.692 \end{bmatrix} \begin{bmatrix} \Delta T \\ \Delta \epsilon \end{bmatrix} \quad (8)$$

Assuming  $\Delta\lambda_B = \Delta\lambda_C = 10$  pm for the wavelength resolution of OSA, resolution of the sensor was calculated as 0.83 °C and 45.80 μϵ for temperature and strain, respectively.

A comparison table was constructed to compare sensitivity of the proposed sensor with the sensors which can perform simultaneous measurement of strain and temperature. Table 1

reveals that proposed sensor exhibits higher sensitivity than Refs. [1, 2, 5, 18, 19] and Refs. [3, 6, 12, 18, 19, 20] in terms of strain and temperature, respectively, and almost the same characteristics with Ref. [10].

TABLE 1. Comparison of sensitivity.

Sensor [ Ref ]	Sensitivity ( $\text{pm}/\mu\epsilon$ )	Sensitivity ( $\text{pm}/^\circ\text{C}$ )
1	0.48	52.00
2	-0.84	-243.40
3	2.57	8.50
5	-0.55	49.60
6	54.97	14.71
10	1.03	57.50
12	-23.70	16.56
18	0.65	40.17
19	0.76	13.20
20	-1.86	9.70
Proposed sensor	1.00	49.92

However, Refs. [4, 9, 13] require expensive and complex equipments to fabricate the sensor and Refs. [7, 8, 16] involve special type fibers so these drawbacks limit their practical use. Consequently, proposed sensor is much easier to fabricate, less expensive, based on standard telecom fiber and needs easier experimental setup compared to dual-parameter sensors available in the literature.

#### 4. CONCLUSION

An easy MZI concatenating a UTF and a DTF for simultaneous measurement of strain and temperature was investigated and demonstrated experimentally. Experimental results indicated that strain resolution of  $9.9 \text{ pm}/\mu\epsilon$  and temperature resolution of  $0.2 \text{ }^\circ\text{C}$  were achieved for discrete measurements. For simultaneous measurements, resolutions of  $0.83 \text{ }^\circ\text{C}$  and  $45.80 \mu\epsilon$  were calculated by using coefficient matrix for temperature and strain, respectively. The thinnest waist diameter is  $65 \mu\text{m}$  so the interferometer is extremely robust. Besides, compactness of the interferometer is provided without including any splicing joint in sensor structure. The interferometer is all-fiber type, cost effective, simple to fabricate and provides high resolution, in that respect, it can be a good choice in simultaneous measurements of strain and temperature in extensive applications.

**Acknowledgments.** This research did not receive any specific grant from funding agencies in the public, commercial, or not-for-profit sectors. Also, the authors would like to thank Net System Infrastructure Services Co. for their support.

REFERENCES

- [1] Sun, H., Yang, S., Zhang, X., Yuan, L., Yang, Z., Hu, M., Simultaneous measurement of temperature and strain or temperature and curvature based on an optical fiber Mach-Zehnder interferometer, *Opt. Comm.*, 340 (2015), 39-43.
- [2] Zhou, D. P., Wei, L., Liu, W. K., Liu, Y., Lit, J. W. Y., Simultaneous measurement for strain and temperature using fiber Bragg gratings and multimode fibers, *App. Optics.*, 47 (2008) 1668-72.
- [3] Jiang, N., Zhu, H., Bao, K., Hu, Y., Simultaneous discrimination of strain and temperature using dual-gratings in one fiber, *Optik*, 126 (2015) 3974-7
- [4] Yang, W., Geng, T., Yang, J., Zhou, A., Zhaojun, L., Geng S., Yuan, L., A phase-shifted long period fiber grating based on filament heating method for simultaneous measurement of strain and temperature, *J. Opt.*, 17 (2015), 1-6.
- [5] Yoon, M. S., Park, S., Han, Y. G., 2012 Simultaneous measurement of strain and temperature by using a micro-tapered fiber grating, *J. Ligh. Tech.*, 30 (2011) 1156-60
- [6] Li, J., Yang, S., Zhang, W., Gao, S., Bai, Z., Wang, L., Liang, H., Yan, T., Simultaneous force and temperature measurement using S fiber taper in fiber Bragg grating, *IEEE Phot. Tech. Lett.*, 26 (2014), 309-312.
- [7] Chu, J., Shen, C., Qjan, F., Zhong, C., Zou, X., Dong, X., Jin, Y., Wang, J., Gong, Y., Jiang, T., Simultaneous measurement of strain and temperature based on a long-period grating with a polarization maintaining fiber in a loop mirror, *Opt. Fib. Tech.*, 20 (2014), 44-47.
- [8] Frazao, O., Marques, L. M., Santos, S., Baptista, J. M., Santos, J. L., Simultaneous measurement for strain and temperature based on a long-period grating combined with a high-birefringence fiber loop mirror, *IEEE Phot. Tech. Lett.*, 18 (2006), 2407-2409.
- [9] Chen, H. F., Wang, D. N., Wang, Y., Simultaneous strain and temperature sensing using a slightly tapered optical fiber with an inner cavity, *Analyst*, 140 (2015), 1859-1862.
- [10] Dong, B., Peng, Y., Wang, Y., Yu, C., Mode division multiplexing in a fiber modal interferometer for dual-parameters measurement, *IEEE Phot. Tech. Lett.*, 28 (2016), 143-146.
- [11] Zhou, J., Liao, C., Wang, Y., Yin, G., Zhong, X., Yang, K., Sun, B., Wang, G., Li, Z., Simultaneous measurement of strain and temperature by employing fiber Mach-Zehnder interferometer, *Opt. Exp.*, 22 (2014), 1680-1686.
- [12] Andre, R. M., Biazoli, C. R., Silva, S. O., Marques, M. B., Cordeiro, C. M. B., Frazao, O., Strain-temperature discrimination using multimode interference in tapered fiber, *IEEE Phot. Tech. Lett.*, 25 (2013), 155-158.

- [13] Zhang, C., Lu, P., Liao, H., Ni, W., Fu, X., Jiang, X., Liu, D., Zhang, J., Simultaneous measurement of axial strain and temperature based on a Z-Shape fiber structure, *IEEE Phot. J.*, 9 (2017), 1-9.
- [14] Navruz, I., Ari, F., Bilsel, M. and AL-Mashhadani, Z. A., Enhancing refractive index sensitivity using micro-tapered long-period fiber grating inscribed in biconical tapered fiber, *Opt. Fib. Tech.*, 45 (2018), 201-207.
- [15] Ghatak, A., *Optics* (4<sup>th</sup> Ed.), Tata McGraw-Hill, 2009.
- [16] Chen, L. X., Huang, X. G., Li, J. Y., Zhong, Z. B., Simultaneous measurement of refractive index and temperature by integrating an external Fabry-Perot cavity with a fiber Bragg grating, *Rev. Sci. Inst.*, 83 (2012), 053113.
- [17] Serway, R. A., Jewett, J. W., *Physics for Scientist and Engineers* (6<sup>th</sup> Ed.), Thomson Brooks/Cole, 2004.
- [18] Qi, T., Xiao, S., Shi, J., Zhou, Z., Bi, M., Li, P., Simultaneous strain and temperature measurement using compact core-offset inter-modal interferometer with embedded fiber Bragg grating, *Asia Communications and Photonics Conference ACP*, Guangzhou, China (2012).
- [19] Hu, Q., Wang, P., Rao, B., Wang, M., Wang, Z., Xu, X., Simultaneous measurement of temperature and strain using double-cladding fiber based hybrid Bragg grating, *OSA Cont.*, 4 (2020), 1031-1037.
- [20] Naeem, K., Chung, Y., Kim, H., Cascaded two-core PCFs-based in-line fiber interferometer for simultaneous measurement of dtrain and temperature, *IEEE Sensors J.*, 19 (2019), 3322-3327.